MSc THESIS

USING MICROMODEL EXPERIMENTS AND IMAGE PROCESSING TO OBTAIN AND ANALYZE THE GRADIENT AND LENGTH OF A PROPAGATING SOLUTE FRONT THROUGH A SATURATED POROUS MEDIUM.

Author:

Joris Dekker

Supervisors:

dr. A. Raoof

Enno de Vries

Department of Earth Sciences
Utrecht University

February 1, 2019

Abstract

Groundwater contamination is an important global problem and therefore a subject of many scientific researches. Many of these research focus on dispersion of a solute on a macro scale. However, pore scale processes can not be neglected, especially when it comes to chemical reactions. The aim of this study is to analyze the effect of porosity and flow rate on a solute front moving through a saturated porous medium on pore scale. This was done by analyzing grey scale images from different micromodel experiments with different flow rates (0.05, 0.1, and 0.2 ml hr^{-1}) and different porosities (0.435, 0.494 and 0.551). Image processing tools were used to obtain the surface area, mean concentration gradient and the length of the solute frontline perpendicular to the flow direction. Results show that for an increase in porosity the frontline length and mean concentration gradient decreases while the total surface area stays almost the same. Results related to different porosity values are less convincing, although a lower mean gradient and shorter solute frontline length were observed for higher porosities.

Contents

1 Introduction **1**

1.1 Solute transport in saturated flow 1

1.2 Pore scale mixing 1

1.3 Micromodel experiments and image processing 2

1.4 Objective of this research 2

2 Methods **3**

2.1. The micromodel experiments 3

2.2. Image filtering 3

2.3. Convert the greyscale images to concentration images 4

2.4. Extract gradient images from the concentration images 5

2.4.1 Resizing and smoothing of the images in MATLAB 5

2.4.2 Create and analyze gradient images with Paraview 5

2.4.2.1 Defining the solute front 6

2.4.2.2 Calculating the mean concentration gradient of the solute front 7

2.5. Obtaining the length of the solute frontline 8

3 Results **10**

3.1. Analysis on the dependency of the concentration front propagation and mean concentration gradient on the flow rate 10

3.1.1 Sensitivity of the mean gradient on the extent of the solute front 10

3.1.2 Influence of flow rate on the length of the solute frontline and the surface area of the solute front 10

3.1.3 Influence of flow rate on mean concentration gradient 11

3.1.4 Influence of flow rate on the surface area of the solute front 12

3.2. Analysis on the dependency of the concentration front propagation and mean concentration gradient on porosity 15

3.2.1 Influence of porosity on solute frontline length and mean concentration gradient 15

3.2.2 Influence of porosity on the surface area of the solute front 17

3.2.3 Discussion on the porosity analysis 17

4 Conclusion **18**

Appendix **20**

References **22**

1. Introduction

Groundwater contamination is an important global problem and therefore a subject of many scientific researches. Knowledge about the spreading of contaminants through a porous aquifer is very useful to predict the extent of a contamination plume, but it can also be used in various medical and industrial applications. The most important processes that cause spreading of solutes through porous media are advection, dispersion and diffusion.

1.1 Solute transport in saturated flow

For a one-dimensional flow, conservative solute transport can be described with the advection and dispersion equation (Bear and Cheng, 2010):

$$\frac{\partial C}{\partial t} = D_L \frac{\partial^2 C}{\partial x^2} - u \frac{\partial C}{\partial x} \qquad (1)$$

Where $\frac{\partial C}{\partial t}$ is the change in concentration over time [MT^{-1}], D_L the longitudinal dispersion coefficient in the flow direction [L^2T^{-1}], u the pore velocity [LT^{-1}], x is the length in the flow direction [L] and C is the concentration [ML^{-3}].

The part of this equation containing D_L is called Fick's law and describes the dispersion of the solute. For this law, diffusion and dispersion are lumped into one dispersion coefficient D which is given by (Bear, 1988):

$$D_L = D_e + a_L v \qquad (2)$$

Where D_e is effective diffusion coefficient [L^2T^{-1}], a_L the longitidunal dispersivity [L] and v the average flow velocity [LT^{-1}].

The relative effect of dispersion over diffusion can be quantified with the Peclet number Pe which will be treated in section 3.1. The dispersion coefficient D_L describes the spreading of a contaminant on a macro scale and by assuming a homogenous porous medium. It can be obtained by fitting breakthrough data as performed by Raaijmakers (2018). According to a statistical analysis performed by Xu and Eckstein (1997) using data from 113 column tests, dispersion depends mostly on porosity and uniformity of the grain size. They also found that the influence of median grain size is only significant for homogeneous porous media.

1.2 Pore scale mixing

At large spatial scales, diffusion can often be neglected because the diffusive part in the dispersion coefficient is much smaller than the dispersive part (Gramling et al., 2002). However, on pore scale, heterogeneity of the porous medium causes distortion of the solute plume (Anna et al., 2013). Anna et al. (2013) and Jiménez-Martínez et al. (2015) found that when a solute is injected in a saturated porous medium, it initially solute starts to form fingers due to the heterogeneity of the porous medium and subsequently variability in flow velocities. During this regime, the spreading of the solute can not be described with Fick's law. This is especially important when it comes to chemical

reactions, because some reactions are depending on pore scale mixing. It is therefore important to understand pore scale mixing processes. Anna et al. (2013) found that the kinetics of a fast biomolecular reaction are controlled by the geometry of the interface front between the reacting chemicals. This geometry depends on the interaction between dispersion and diffusion and, in some cases, chemical reactions (Dentz et al., 2011). Willingham et al. (2008) compared pore-scale numerical simulations with micromodel experimental data for mixing and mixing limited chemical reactions. They found a good agreement between the results from the simulation and the results from the experiments.

1.3 Micromodel experiments and image processing

In this research, experimental data from micromodel experiments performed by Raaijmakers (2018) were analyzed using different image processing tools. There is no clear definition of a micromodel, but Karadimitriou and Hassanizadeh (2012) defined them as 'an artificial representation of a porous medium made of transpartant material'. Micromodels typically have an overall size on the centimeter scale and are a valuable tool for studying the pore scale behavior of fluids (Karadimitriou and Hassanizadeh, 2012). Micromodels do exist as of approximately 1952, when Chatenever and Calhoun (1952) used them to investigate microscale mechanism of fluid behavior in Porous media. Their micromodel had a simple and regular geometry, but micromodels with a more complicated geometry have been constructed over the years (Karadimitriou and Hassanizadeh, 2012). Image processing can be used to analyze the data from micromodels experiments. It was used in several two-phase flow studies to determine phase-saturation and interfacial area (Cheng, 2002; Pyrak-Nolte et al., 2008; Cheng et al., 2004; Chen et al., 2007). Anna et al. (2013) and Karadimitriou et al. (2016) also used image processing to convert grey scale images from micromodel experiments to concentration images.

1.4 Objective of this research

This research builds on data from micromodel experiments performed by Raaijmakers (2018) consisting of grey scale images taken every 5 seconds from an ink solution progressing through a saturated micromdoel. Raaijmakers (2018) focused in their analysis on the dependence of dispersivity a on flow rate and porosity. In our research, the same data was used to analyze the geometry of the progressing front of the injected ink solution. This analysis was performed by using different image processing tools. First, the images had to be filtered to remove background noise. This was done using ImageJ software (Rasband, 1997). After the filtering, the greyscale images had to be converted to images containing concentration values. Using Paraview (Kitware, 2000) and Matlab software (The MathWorks Inc., 2018), the mean concentration gradient, surface area and length perpendicular to the flow direction of the propagating solute front were obtained. This was done for three different micromodels with a different porosity but similar pore structure and for three different flow rates in order to investigate the effect of changes in porosity and flow rate on the geometry of the solute front.

2. Methods

2.1. The micromodel experiments

The experiments were performed on micromodels made of polydimethylsiloxane (PDMS) using the soft lithography technique, which is explained in more detail in Karadimitriou et al.(2013). The models were composed of two slabs, one slab was containing a synthetic pore network while the other slab was functioning as a blank cover. The slabs were bounded together by corona discharge. Three micromodels were fabricated with different pore networks and all the micromodels had a size of 10 x 10 x 0.069 mm. The grain distribution and connectivity of the pore networks were the same, but the grain size differed in order to get different porosity values. The pore networks were based on a CT scan of a slice of natural sand packed soil.

Before starting the experiments, the micromodels were saturated with a solution with a known concentration. This was done for 5 different concentration values and for each micromodel. The greyscale images taken of the saturated micromodels were used as calibration images (see section 2.3). For conducting the experiment, the models were first fully saturated with water after which an ink solution was introduced with a constant flow rate for a fixed duration and was flushed with solute-free water. This process of the ink solution imbibing and draining the pore network was captured with a Canon EOS 5DSR camera that was taking images with a speed of 0.2 fps. Experiments were performed on each of the three micromodels with three different flow rates. The process of fabricating the micromodels and the steps that need to be taken in order to make them suitable for the experiments is explained in more detail in Raaijmakers (2018).

2.2. Image filtering

Before being analyzed, the images obtained from the micromodel experiments had to be filtered to remove noise. This filtering was done using Imagej software (Rasband, 1997) and performed on both the images for the experiment and the images with a known concentration value used for calibration. (Raaijmakers, 2018). These calibration images were also used to test the effectiveness of the filters (Table 1). The best results, without smoothing the images too much, were obtained by first applying a 'remove outliers' with a radius of 10 pixels and a threshold value of 5 followed by a 'median' filter with a relatively small radius of 5 pixels. The *remove outliers* filter replaces a pixel with the median of its surrounding with a radius of 5 pixels if the value deviates from the median by more than 5. The *median* filter replaces a pixel with the median value of its surrounding with a radius of 5 pixels. The exact working of these filters is explained in more detail in the Imagej user guide (Ferreira & Rasband, 2012).

Table 1. *Effect of different filters on one of the calibration images (so with one concentration value). The values are greyscale (GS) intensities because the images are not yet converted to concentration images.*

	Mean GS	*Median of GS*	*Standard deviation of GS*
unfiltered	33,66	34	3,31
median filter (radius 15)	33,57	34	1,78
remove dark and bright outliers filters (radius=10 threshold=5)	33,61	34	2,71
remove dark and bright outliers filters (radius=10 threshold=5) followed by a median filter (radius=5)	33,51	34	2,03

2.3. Convert the greyscale images to concentration images

After the filtering, the greyscale images had to be converted to concentration images. A short description of the method used is provided here, a more detailed description can be found in Raaijmakers (2018). First, 5 water-ink solutions with a known concentration value were prepared. For each micromodel and water-ink solution, greyscale images were taken of a fully saturated micromodel with one of the water-ink solutions. These images were used to obtain a relation between the grey scale intensity and concentration. This relation was found to be an exponential function with a form of (Kohl et al, 2006; Raaijmakers, 2018):

$$C = ae^{bI} \qquad (3)$$

Where C being the concentration, I the greyscale intensity and a and b are fitting constants. The pore space -i.e., the area of the image excluding the grains and the edges, of the greyscale images used for calibration and the images of the experiment were divided into regions of 5 by 5 pixels. Because of the irregular size of the pore space, not every region could be exactly 5 by 5 pixels in size. When regions became too small, they were merged together. For each region, the median greyscale intensity was calculated. We have chosen to apply a median filter instead of a mean filter because a median filter excludes the outliers in the region -i.e., cells with a very high or low greyscale intensity compared with the surrounding cells. Using the known concentration values and the median greyscale intensities of the calibration images, each region was fitted to the Equation 3 to get unique values for a and b constants. After this, Equation 3 was applied to the images of the experiment to convert the median greyscale intensity of each region to a concentration value using the fitting constants for that specific region. An example of a concentration image is shown in Figure 1.

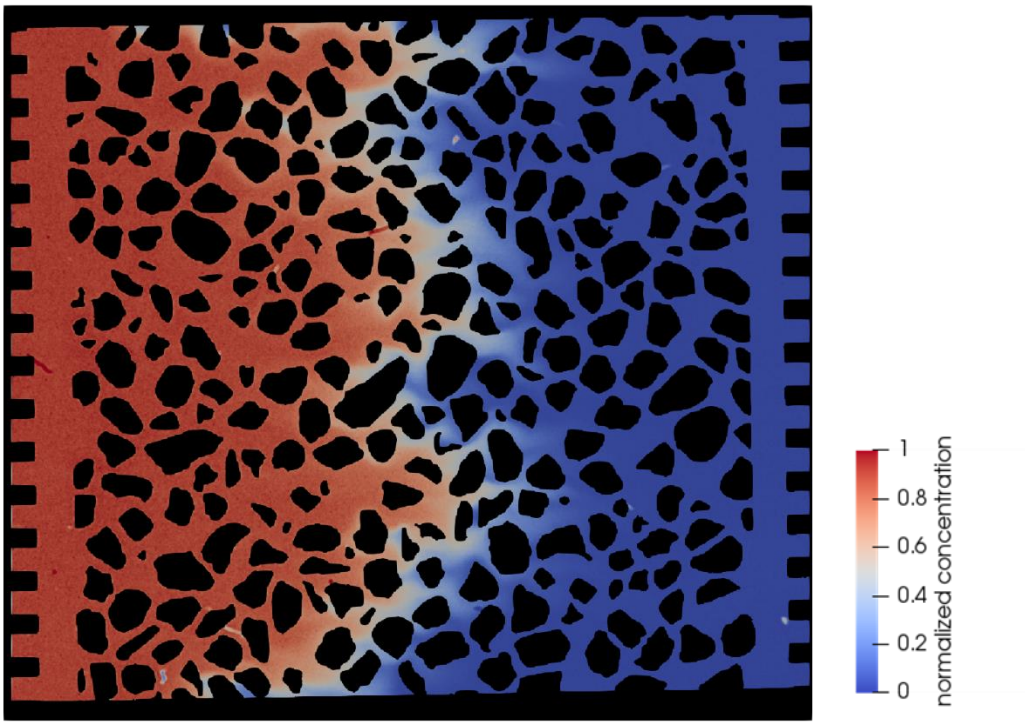

Figure 1. *Concentration image from a micromodel experiment after the conversion from grey scale to concentration. The image is from a micromodel experiment with a porosity of 0.551 and a flow rate of 0.1 ml/hour after 250 seconds of injection of ink-solution.*

2.4. Extract gradient images from the concentration images

The flow and transport regime determines the gradient of concentration at the progressing front. One of the objectives of this research was to examine the temporal evolution of the gradient of the concentration front and how this gradient behaves with different input flow rates and in different micromodels with similar pore structures but different porosities. To do this, several steps had to be taken:

2.4.1 Resizing and smoothing of the images in MATLAB

Because the pore spaces of the concentration images are divided into boxes of 5 by 5 pixels, the gradient is only calculated at the edge of the boxes – i.e., at the boundary with the adjacent box. To prevent this, the images were resized using the *imresize* function of Matlab. The images were resized with a scale of 1/box size, so in this case 1/5=0.2. This resulted in images with a 5 times lower resolution, but with a unique concentration value for each pixel corresponding to the concentration value of the box that the pixel fell in. Of course, this caused some problems with the boxes surrounding the grains because they were mostly smaller than 5 by 5 pixels and could therefore be skipped by the resize function. However in this case, because of the relatively small box size this caused no major problems. Figure 2 shows the effect that the *imresize* function has on the concentration images. As can be seen, only the pixels surrounding the grains are affected.

Another problem is that often the pixels surrounding the grains (i.e., pixels just next to the grains) have concentration values that differ significantly with the surrounding. These deviations are probably caused by very small shifting/movement of the images during the experiments. To exclude these pixels, a median filter was performed with a neighborhood size of 3 by 3. This filter smoothens the images and replaces the pixels around the grains with NaN (not a number) values. After this, all the NaN values were replaced by a minus value, because Paraview software cannot handle NaN values in VTK files. The grain cells can then easily be filtered out using the *threshold* filter.

Finally, both the smoothened as the unsmoothed images were converted to vtk files using the Matlab script vtkwrite (Joe Yeh, 2016) and imported into Paraview (Kitware, 2000) for further analysis.

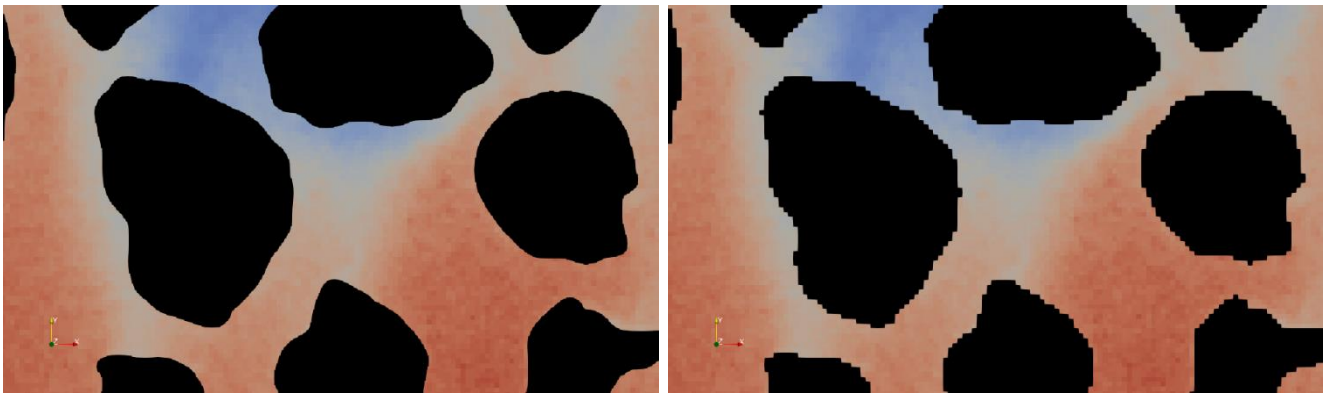

***Figure 2**. Before and after image showing the effect of the the imresize function of Matlab. The left image is before resizing, the right image is after resizing. As can be seen, only the cells surrounding the grains are affected.*

2.4.2 Create and analyze gradient images with Paraview

The concentration gradient is defined as the change in concentration over an infinitely small distance in a certain direction. Because each cell in the concentration images has a certain concentration value, image processing can be used to calculate the mean concentration gradient. This works as

follows: for each cell the difference between that cell and its adjacent cells is calculated. From this, the gradient magnitude of that cell can be obtained. The mean gradient can then be calculated by adding the gradients of all the cells together and dividing them by the number of cells. Below is a description of the steps that have been taken in Paraview to get a mean gradient value of the concentration front.

2.4.2.1 Defining the solute front

First, the solute front had to be defined. A *threshold* filter was applied on the unsmoothed images excluding all the concentration values above 0.6 - i.e., only the concentration values between 0.0 and 0.60 remained. As can be seen in the Figure 3, several isolated spots of lower concentration are still present that are not part of the concentration front. Some of these spots are the result of noise in the images that was not filtered out, others are isolated regions of immobile water zones where grains prevent the inflow of solute. An easy way to filter these spots out is by applying a *connectivity* filter. This filter divides the image into regions each having one set of connected cells and extracts the largest region, thereby removing the small groups of connected cells that are not connected with the right boundary of the micromodel (Figure 3).

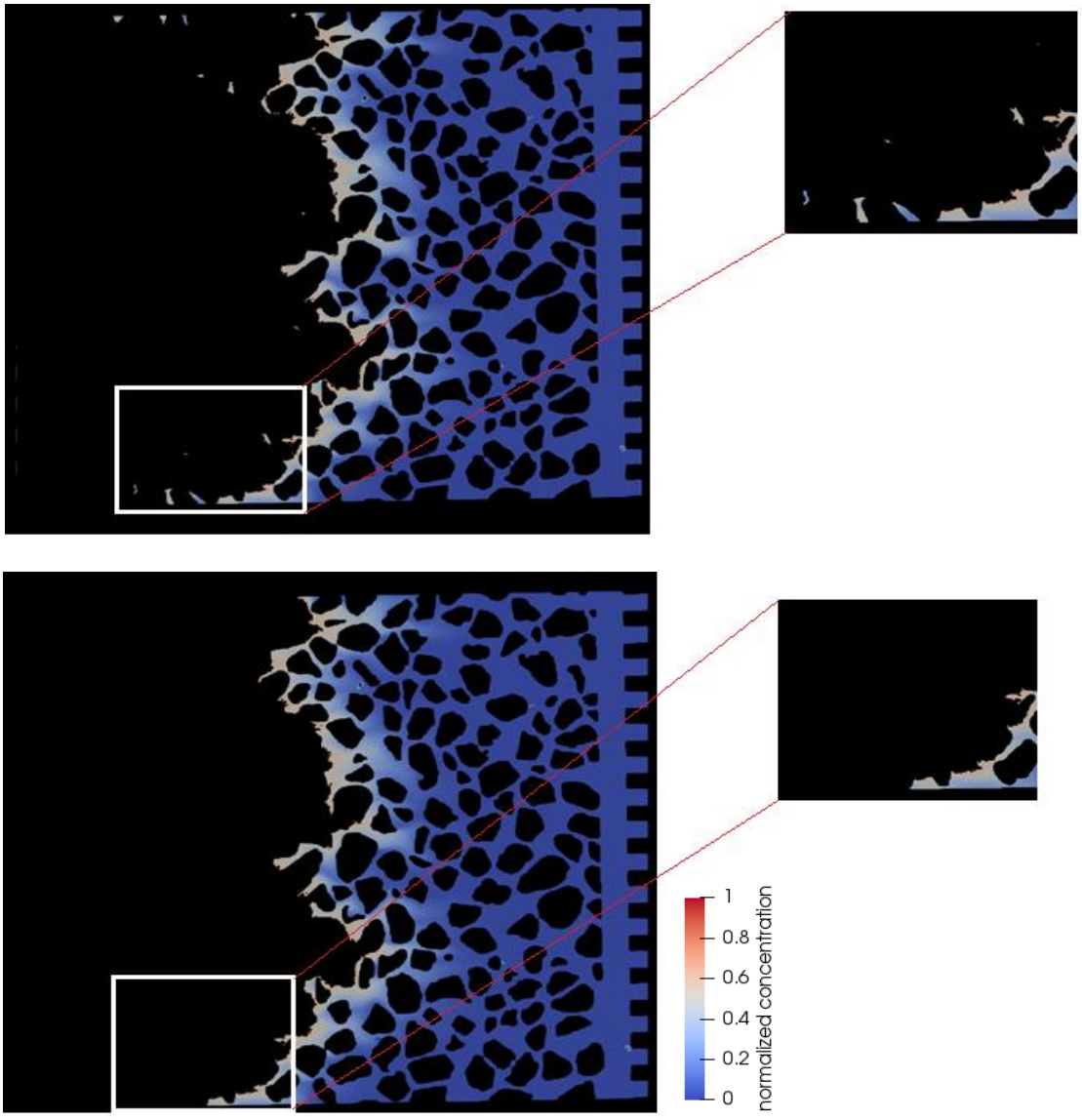

Figure 3. *The solute front before (top) and after (bottom) the Connectivity filter. The grey area consists of both grains and concentration that is not part of the defined front (so C > 0.6). The images are from a micromodel experiment with a porosity of 0.551 and a flow rate of 0.1 ml/hour.*

After this, the smoothened images were used to mask out the deviating concentration values on the edge of the grains and a new threshold was applied to extract the pixels with a concentration value between C_{min} and C_{max} -i.e., the concentration values between which the solute front is defined. This provides the area over which the mean gradient will be taken (Figure 4). To analyze the effect of the extent of the solute front on the mean gradient, three different values of the C_{min} were used while C_{max} was kept constant at 0.6. The results of this analysis will be discussed in section 3.1.

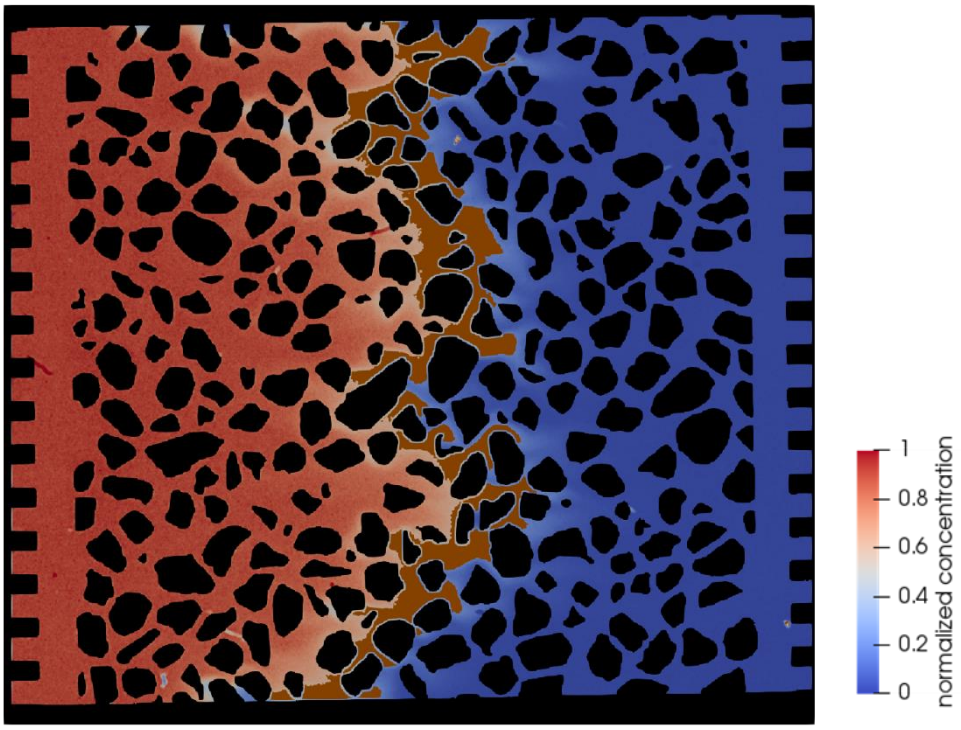

***Figure 4**. The solute front (brown area) containing concentration values between 0.2 and 0.6. The image is from a micromodel experiment with a porosity of 0.551 and a flow rate of 0.1 ml/hour*

2.4.2.2 Calculating the mean concentration gradient of the solute front

The Paraview *gradient* filter was used to calculate the concentration gradient for each pixel within the concentration front. This filter uses the central difference gradient method, which means that the gradients of a pixel in the discrete x and y direction are defined as:

$$\frac{dC}{dx} = (C(x_i + 1) - C(x_i - 1))/2 \qquad (4)$$

$$\frac{dC}{dy} = (C(y_j + 1) - C(y_j - 1))/2 \qquad (5)$$

From these directional gradients, the gradient magnitude can be calculated as follows:

$$g = \sqrt{((\frac{dC}{dx})^2 + (\frac{dC}{dy})^2)} \qquad (6)$$

The Paraview *gradient* filter was applied to the cells that fell within the solute front. The mean gradient magnitude of these cells was calculated and plotted over time. A similar method was used by Jiménez-Martínez et al. (2015) to get the mean concentration gradient over a diffusive mixing interface. In our case, the highest gradients were found at the direction transverse to the flow which is caused by the forming of solute fingers at the beginning of the injection due to preferential flow paths. (Figure 5).

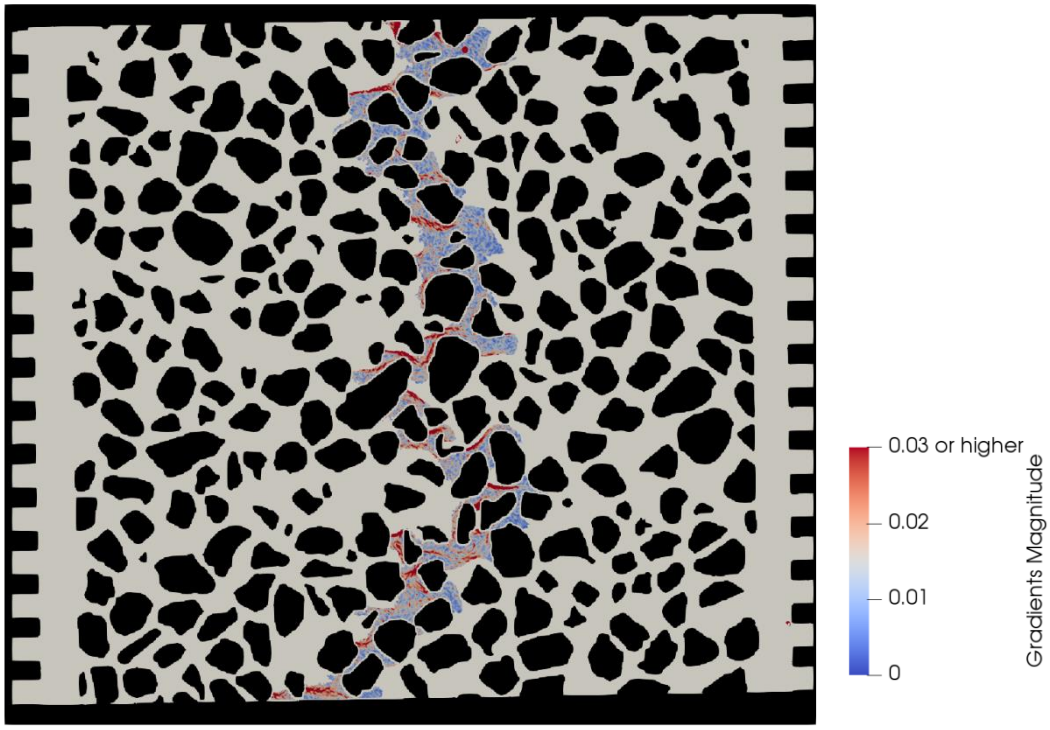

Figure 5*. Results of the Paraview gradient filter applied to the solute front of a micromodel experiment with a porosity of 0.551 and a flow rate of 0.1 ml/hour of . Areas of high gradients are mostly oriented along the flow direction.*

2.5. Obtaining the length of the solute frontline

Another object of this research was to examine the length of the solute frontline perpendicular to the flow -i.e., the tortuosity of the solute frontline. The frontline was defined as a contour line that represents a normalized concentration value of 0.5. To get this line, the solute front with normalized concentration values between 0.4 and 0.6 was defined using the method described in the previous sections. The frontline was obtained using the *contour* filter of Paraview. To make sure that the frontline becomes a smooth line, first a median filter with a neighborhood size of 5 by 5 was performed on the concentration images. Because it is only possible to define a contour line in the pore space, the *contour* filter resulted in isolated lines between the grains (Figure 6a). Adding up the length of these lines and plotting them over time did not give good results due to the heterogeneity of the pore network. Therefore, a Matlab script was created that connects the isolated contour lines and create one frontline. Working from the upper boundary to the lower boundary, the distances of both ends of each contour line to the ends of the other contour lines were calculated. The contour line was then connected to the contour line that has the shortest distance to it (Figure 6b). It was made sure that no end of a contour line was used more than once. The assumption was made that the isolated contour lines were connected to each other by straight lines. The results were compared

to the concentration images and corrected manually when contour lines were not connected correctly by the Matlab script (Figure 6c).

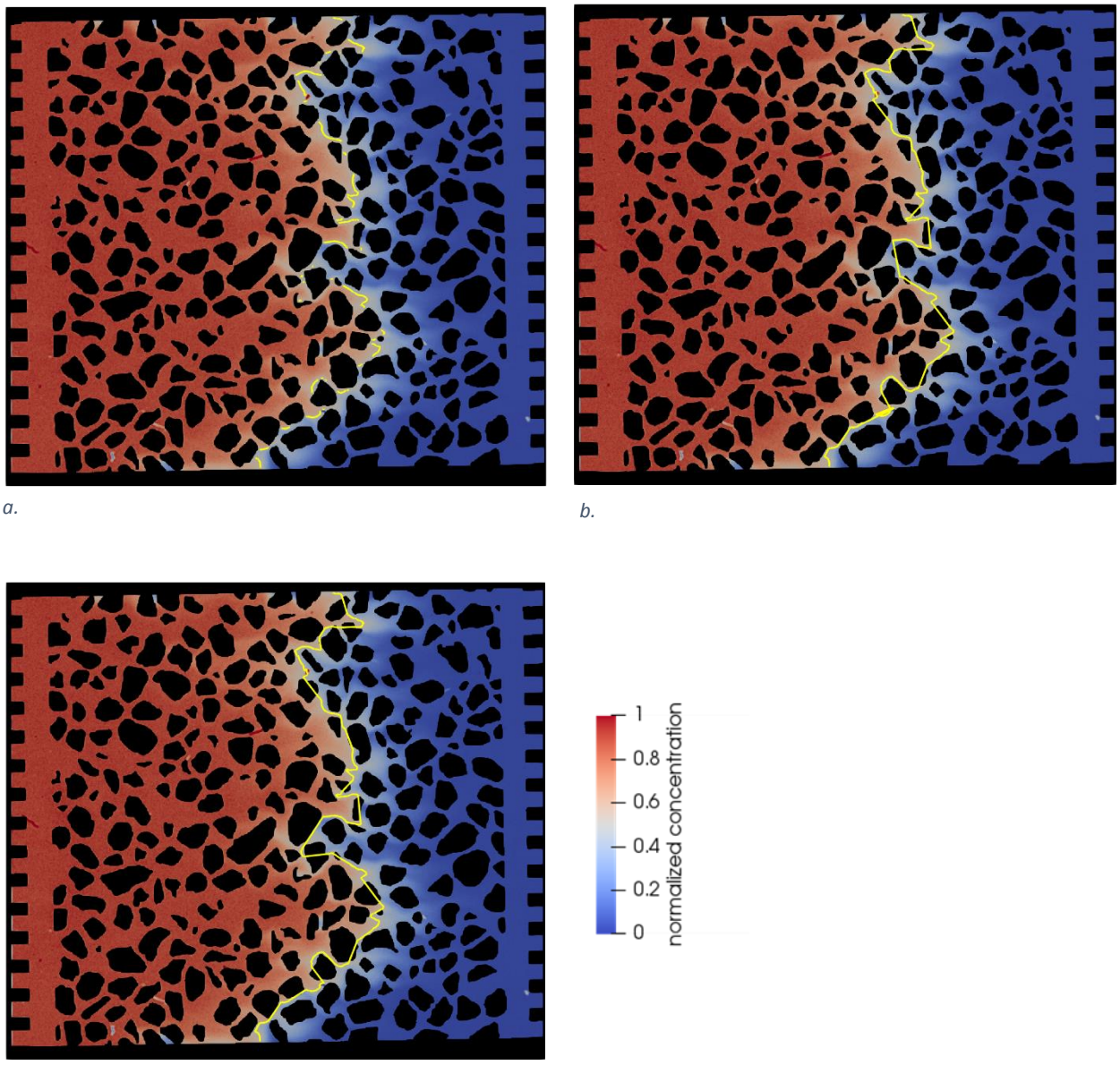

a. *b.*

c.

Figure 6. *The yellow line represents respectively: (a) the contour line created by the Paraview contour filter (b) the isolated contour lines connected with straight lines based on the shortest distances between the lines (c) the contour lines connected based on the shortest distances and corrected manually. The images are from a micromodel experiment with a porosity of 0.551 and a flow rate of 0.1 ml/hour*

3. Results

3.1. Analysis on the dependency of the concentration front propagation and mean concentration gradient on the flow rate

The methods described in section 2 were used to analyze data obtained by microfluidic solute transport experiments. Experiments have been done on 3 different porous media where the porosity was varied by reducing the grain sizes. For each porous media the input flow rate was varied 3 times, so in total 9 microfluidic experiments were done. For this research, 5 of these experiments were analyzed including experiments with one porosity and different flow rates and experiments with one flow rate and different porosities. The mean gradient and length of the solute frontline were calculated between the moment the solute enters the porous medium and the moment the solute front leaves the porous medium. For the mean concentration gradient, the extent of the defined solute front -i.e., the area over which the mean gradient was taken, was varied to examine how this influenced the results.

3.1.1 Sensitivity of the mean gradient on the extent of the solute front

Figure A1 in the appendix shows the mean concentration gradients of the solute front plotted against time. It seems that a larger range of concentration values that are defined as part of the solute front leads to a less scattered graph. An explanation for this is that the when mean is taken over more cells, the influence of deviating gradient values caused by noise in the image and inaccuracy of the gradient filter decreases. Therefore, a front range of concentration values between 0.2 and 0.6 was chosen for the mean concentration gradient calculation and the surface area of the solute front.

3.1.2 Influence of flow rate on the length of the solute frontline and the surface area of the solute front

Figure 8 shows the movement of the solute front through the porous medium for a flow rate of 0.1 ml/hour. For all flow rates, fingers start to form when the solute enters the pore network due to the heterogeneity of the flow which leads to an increase in length of the solute frontline. After a while, diffusion leads to merging of the formed solute fingers and therefore a decrease in length of the solute frontline can be observed. The forming of early time fingers when a solution enters a porous medium was also observed by Anna et al. (2013) and Jiménez-Martínez et al. (2015). Figure 7 shows the surface area of the solute front plotted against Pore Volume for different flow rates. The graph shows a linear increase in surface area for all flow rates after a Pore Volume of 0.5. The steep increase in surface area before a Pore Volume of 0.5 is caused by the introduction of the solute in the porous medium. Surprisingly, the flow rate seems to have no significant influence on the evolution of the frontal surface area. A possible explanation for this will be given later. The length of the solute frontline is plotted in figure 9. Initially, the length of the frontline increases due to the forming of solute fingers. When the fingers start to merge due to diffusion, the length of the frontline seems to decrease. It is important to note that the pore structure of the micromodel has a large influence on the results due to the method by which the frontline length was calculated. Nevertheless, despite the inaccuracy of this method, the increase in length of the frontline until a pore volume of approximately 1.2 is clearly visible for all flow rates and is in agreement with experimental results obtained by Anna et al. (2013). Table 3 shows the mean maximum frontline length for all flow rates. This is defined as the frontline length averaged over the time period between a Pore Volume of 1 and 1.5, which is the period that the frontline reaches its maximum length.

An increase in mean maximum frontline length of approximately 2.4 mm can be observed when the flow rate is doubled. This is caused by an increasing influence of dispersion over diffusion which can be explained by the Peclet number. The Peclet number is defined as (Freeze & Cherry, 1979):

$$Pe = \frac{vd}{D_e} \qquad (7)$$

where v is the average flow velocity [LT^{-1}], d is the characteristic length of the porous medium [L] and D_e is the effective diffusion coefficient [L^2T^{-1}]. The Peclet numbers of the experiments are shown in table 2 (Raaijmakers, 2018).

Table 2. Peclet numbers of the micromodel experiments obtained by Raaijmakers (2018). The porosity values of the models are shown between brackets

Flow rate	*Model 1 (0.435)*	*Model 2 (0.494)*	*Model 3 (0.551)*
0.05	18.9	17.3	15.4
0.1	37.8	32.6	30.2
0.2	70.5	64.0	59.3

The larger the Peclet number, the larger is the effect of dispersion over diffusion. So, in case of a higher flow rate and thereby a higher average flow velocity through the porous medium, the Peclet number is higher. This indicates that the effect of dispersion over diffusion on the movement of the solute is higher. Therefore, there is less merging of solute fingers and the frontline will become longer because the solute front will become more stretched out in the direction of the flow.

3.1.3 Influence of flow rate on mean concentration gradient

Figure 11 shows a linear decrease of the mean concentration gradient with time for all the flow rates after a Pore Volume of 0.5. For all flow rates, the decrease of the mean gradient ceases after some time and the mean gradient remains almost constant until the solute reaches the end of the porous medium. However, Jiménez-Martínez et al. (2015) found that the gradient will likely decrease further after the constant period for longer timescales. The moment that the mean concentration gradient ceases to decrease seems to coincide with the moment that most of the concentration fingers are merged and the frontline length does not increase any longer (Figure 9 and 11). It is important to note that the gradient started to decrease during the period before the solute reaches the pore network due to the inlet structure, which is the reason for the steep decrease at the beginning of the graphs (Figure 11).The mean gradient only depends on diffusion during this period, so the slope of the decrease in mean concentration gradient is much higher for a lower flow rate because the solute has more time to diffuse. Consequently, the mean concentration gradient is not the same for each flow rate at the moment the solute enters the pore network. As soon as the solute enters the pore network, dispersion starts to take place and the slope of the decrease in mean gradient clearly decreases for all flow rates. From this moment on, the graph for a flow rate of 0.05 ml/hour shows the least steep slope. As can be seen in figure 10, areas of high concentration gradients are mostly oriented along the flow direction which is in indication that the highest concentration gradients can be found at the edges of the solute fingers and transverse to the flow direction. As previously shown, a higher flow rate leads to a more stretched solute front - i.e., a longer front line and therefore larger areas of high mean concentration gradient at the edges of the solute fingers. Presumably, this slows

down the decrease in mean gradient and explains the less steep slopes for flow rates higher than 0.05 ml/hour (Figure 11). Figure 11 shows that a higher flow rate corresponds to a higher mean concentration gradient when the solute reaches the end of the pore network. The mean concentration gradients at this moment are respectively 0.011, 0.013 and 0.015 for a flow rate of 0.05, 0.1 and 0.2 ml/hour, which means an increase of 0.002 for a twice as high flow rate. It is important to realize that it is not clear in what extent the initial mean gradient of the solute influences the mean gradient of the solute at the end of the pore network. Therefore, new experiments need to be carried out where the initial gradient is kept the same for all flow rates. This can be a subject for future research.

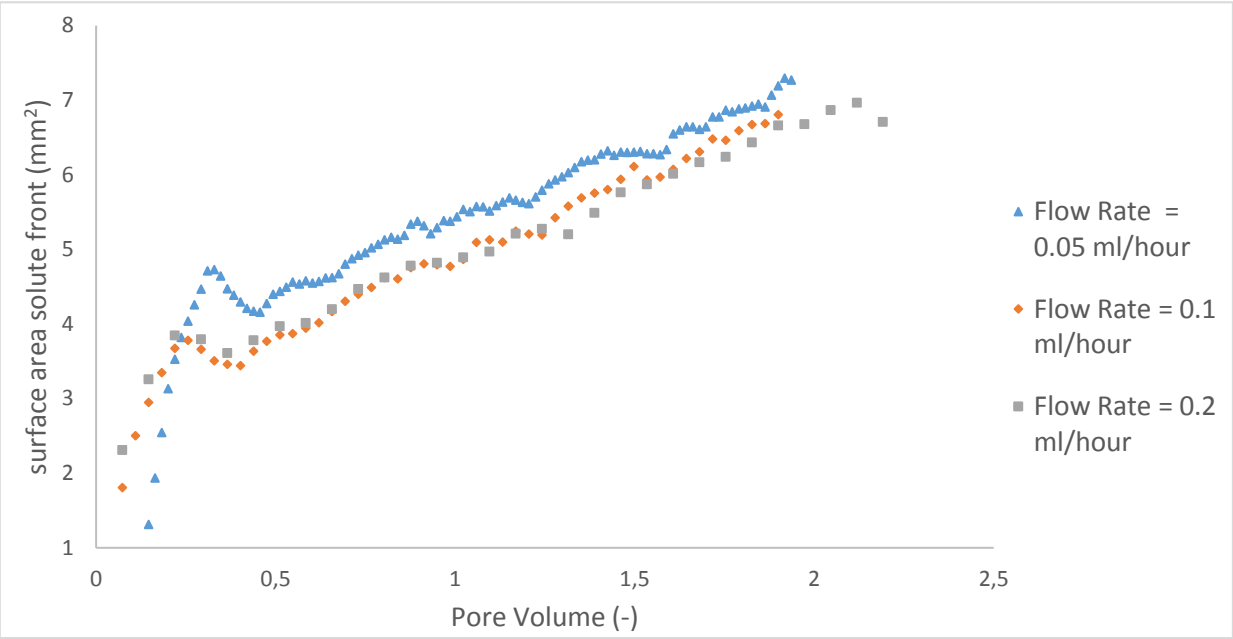

Figure 7. The surface area of the solute front for different flow rates and a porosity of 0.551 plotted against Pore Volume. The surface area of the solute front is defined as the group of cells that contains concentration values between 0.2 and 0.6 and are part of the solute front –i.e., not from isolated spots of deviating concentration values.

3.1.4 Influence of flow rate on the surface area of the solute front

Both dispersion and diffusion lead to an increase in surface area of the solute front. The flow rate has little to no influence on the increase in surface area of the solute front, but it does influence the length of the solute frontline and the mean concentration gradient of the solute front. With an increase in flow rate, an increase in surface area of the concentration front due to a longer front length (more dispersion) is opposed by an increase in mean concentration gradient (less diffusion). Consequently, the differences in surface area of the solute front are minimal between the different flow rates.

Table 3. *Mean maximum solute frontline lengths for different flow rates and a porosity of 0.551.*

Flow rate (ml hr^{-1})	*Mean maximum frontline length (mm)*
0.05	16.41112
0.1	18.82011
0.2	21.14008

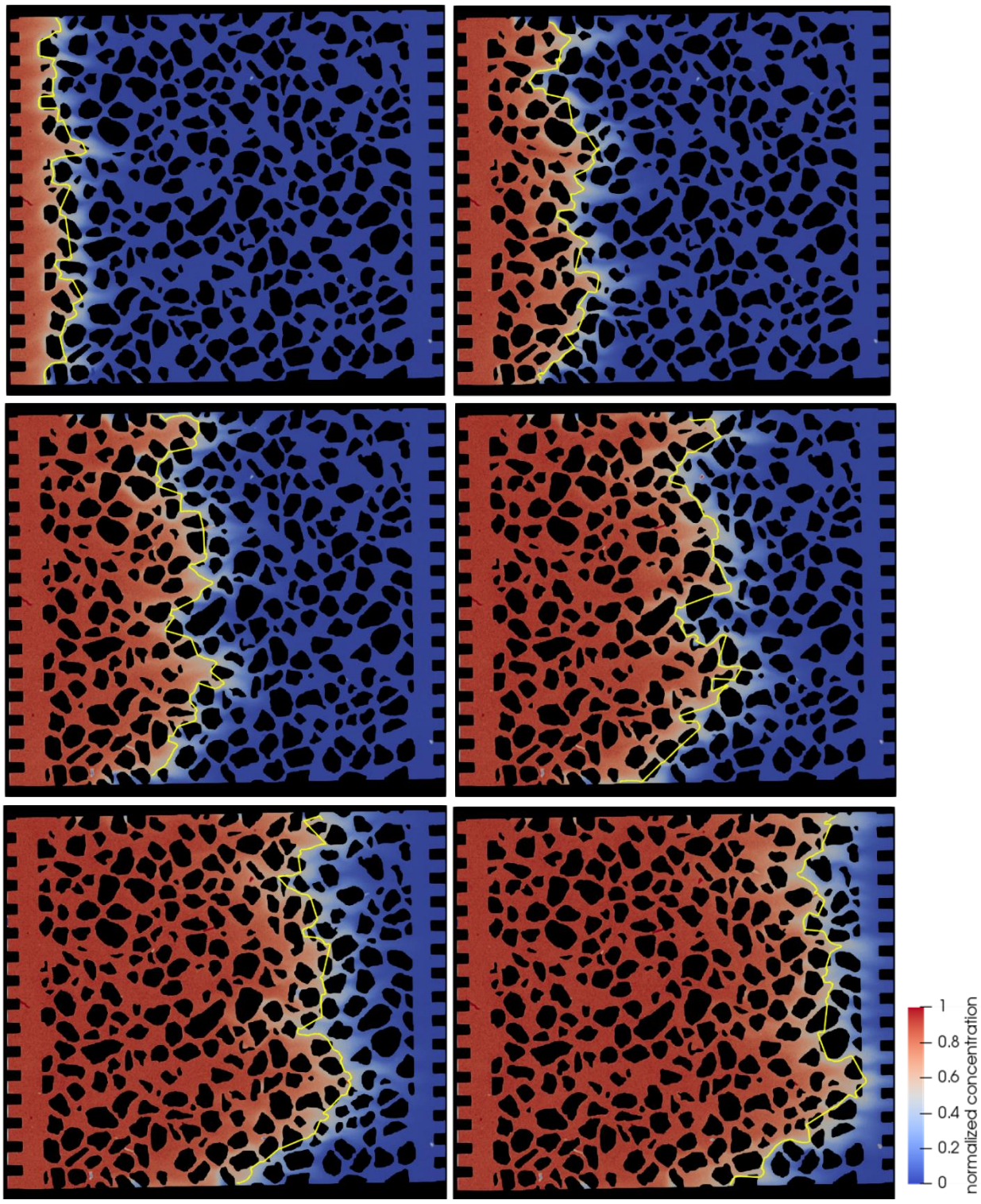

Figure 8. *Concentration images showing the movement of the solute frontline. The images are from the experiment with a flow rate of 0.1 ml/hour and a porosity of 0.551. The yellow line represents the solute frontline.*

Table 3. *Mean maximum solute frontline lengths for different flow rates and a porosity of 0.551.*

Flow rate (ml hr^{-1})	*Mean maximum frontline length (mm)*
0.05	16.41112
0.1	18.82011
0.2	21.14008

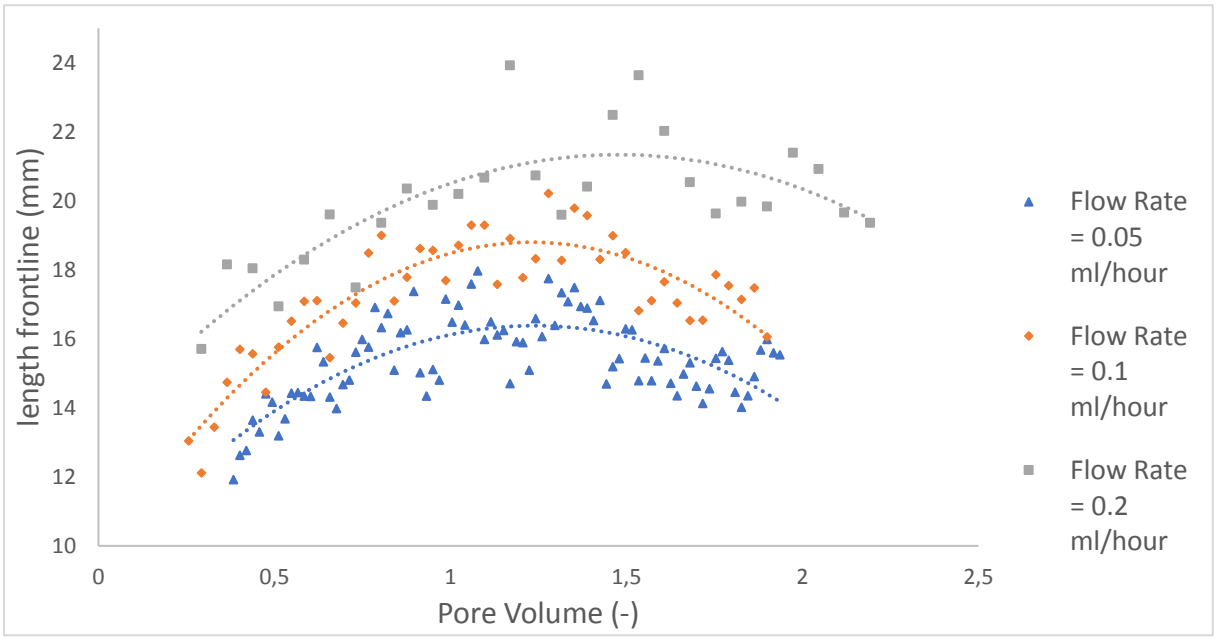

Figure 9. The length of the solute frontline for different flow rates and a porosity of 0.551 plotted against Pore Volume. The dotted lines represent quadratic functions that were fitted through the data.

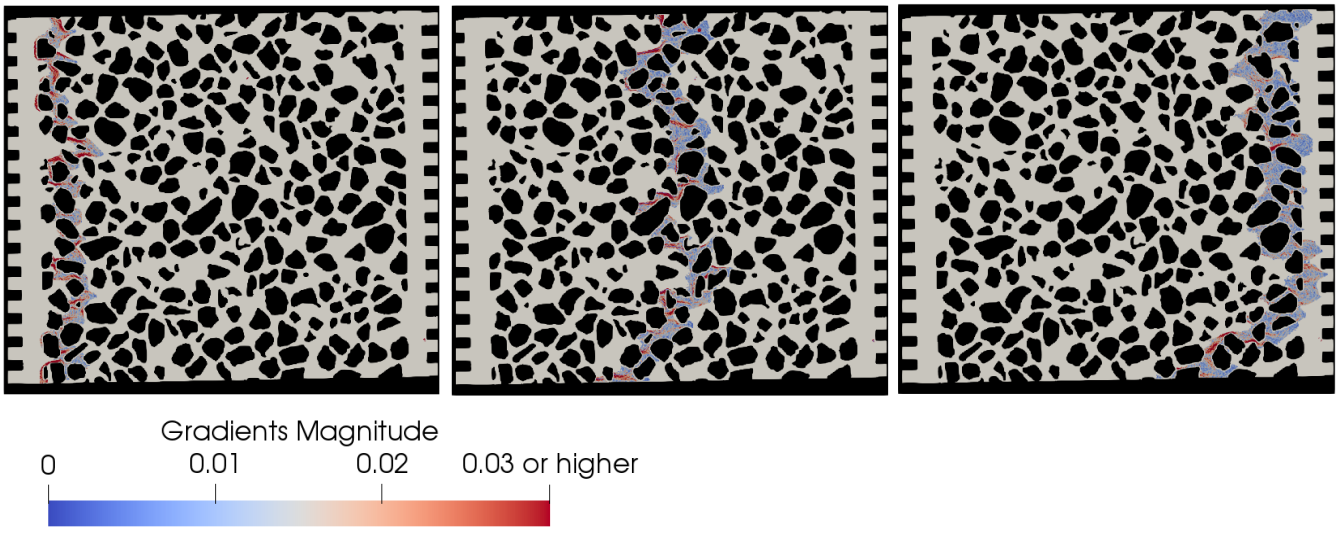

Figure 10. *Images showing the concentration gradients as the solute moves through the pore network for a flow rate of 0.1 ml/hour and a porosity of 0.551.*

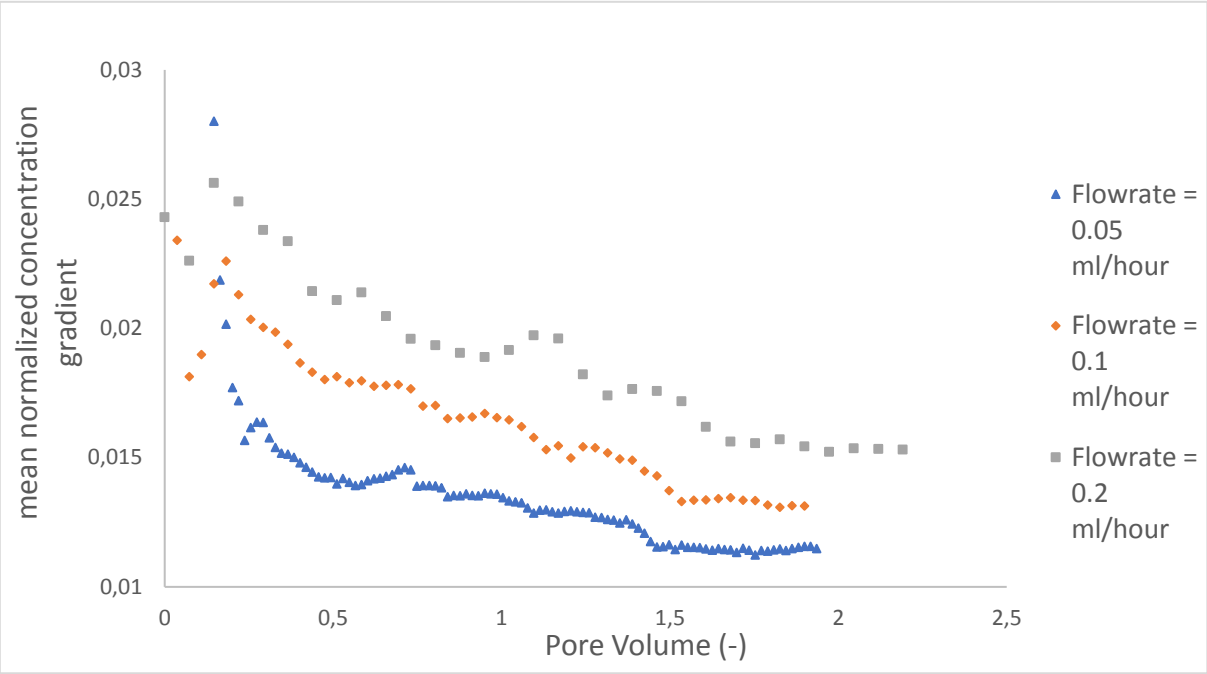

Figure 11. Mean concentration gradients plotted against Pore Volume for different Flow Rates and a porosity of 0.551.

3.2. Analysis on the dependency of the concentration front propagation and mean concentration gradient on porosity

3.2.1 Influence of porosity on solute frontline length and mean concentration gradient

Figure 12 shows images of the three micromodels with a different porosity at the moment the solute front is approximately halfway the pore network. Based on this figure, the length of the solute fingers decreases with an increase in porosity -i.e., the solute front becomes less stretched in the flow direction. This can be explained by the fact a higher porosity leads to a smaller variability of particle velocity -i.e., the velocity of one ink particle, causing a decrease in dispersion. Raaijmakers (2018) found indeed a decrease in dispersivity for an increase in porosity based on the same experiments as in our research. In contrast to experiments with a porosity of 0.551, the mean concentration gradients of the solute front do not seem reach a constant state for a porosity of 0.435 and 0.494 (Figure 14). It is not clear if this can be explained by a lack of measuring points or that the extent of the pore network is too small to reach this constant state. Lower mean concentration gradients can be observed when the porosity increases from 0.435 to 0.493 (Figure 14), while the mean maximum solute frontline length stays almost the same (Figure 13 and Table 4). This indicates that for this change in porosity, the increase in pore space leads to an increase in diffusion because the solute has more space to diffuse. Also, the effect of areas with a high concentration gradient on the mean concentration gradient becomes smaller. The constant mean maximum frontline length shows that this increase in porosity has no significant influence on the amount of dispersion. On the other hand, the mean maximum frontline length clearly decreases when the porosity increases from 0.494 to 0.551 while the evolution of the mean concentration gradient stays almost the same (Figure 14 and Table 4). So for this change in porosity, the smaller variability in particle velocity leads to less dispersion but does not lead to a clear increase in diffusion.

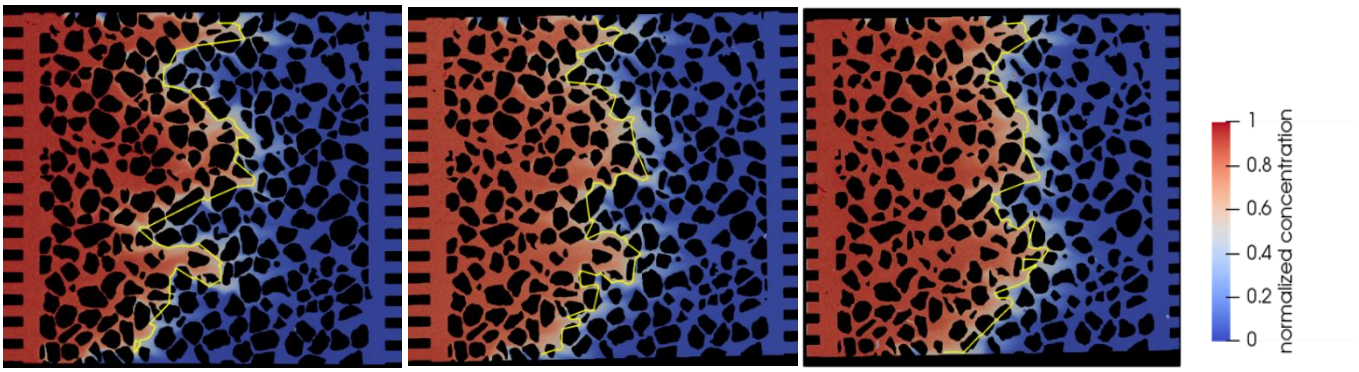

***Figure 12**. Concentration images from three micromodel experiments as the solute is approximately halfway the pore network. The yellow line represents the solute frontline. The porosities of the micromodels are from left to right: 0.435, 0.494 and 0.551.*

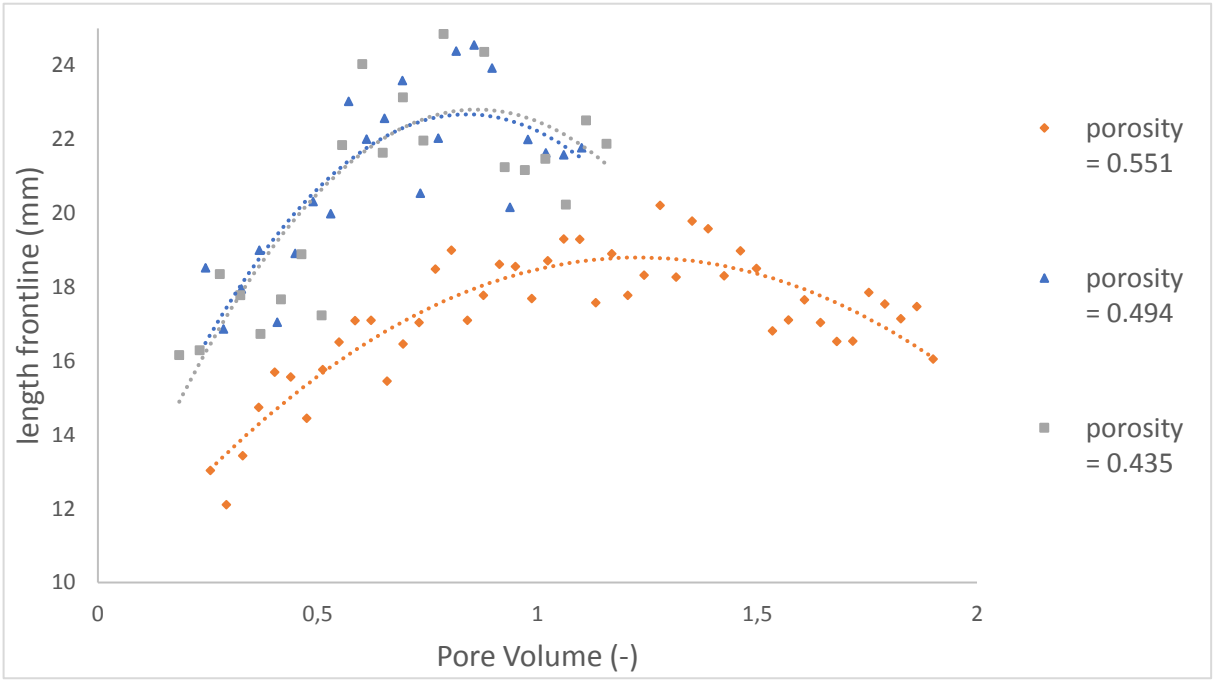

Figure 13. The length of the frontline for different porosities and a flow rate of 0.1 ml/hour plotted against Pore Volume. The dotted lines represent quadratic functions that were fitted through the data.

***Table 4.** Mean maximum front lengths for different porosities and a flow rate of 0.1 ml/hour. For a porosity of 0.551, the mean was taken over the front lengths in the period between a Pore Volume of 1 and 1.5, for a porosity of 0.435 and 0.494 the period between a Pore Volume of 0.5 and 0.9 was used.*

porosity (-)	*Mean maximum frontline length (mm)*
0.435	22.75
0.494	22.66
0.551	18.82

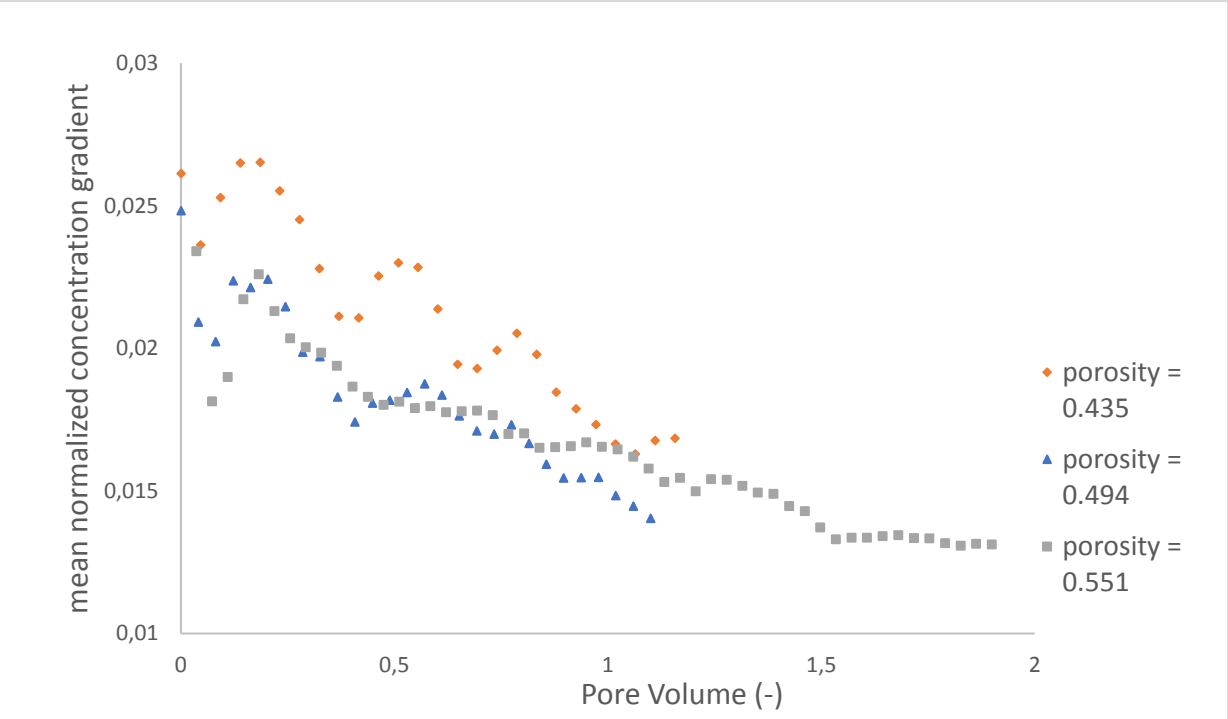

Figure 14. Mean concentration gradients plotted against Pore Volume for different porosities and a flow rate of 0.1 ml/hour.

3.2.2 Influence of porosity on the surface area of the solute front

When looking at the surface area of the solute front, clearly higher values can be observed for a porosity of 0.494 than for the other porosity values (Figure 15). This can be a consequence of an increase in diffusion compared to the results for a porosity of 0.435, which is also backed by a decrease in mean gradient. A decrease in dispersion, indicated by a decrease in mean maximum front length, is probably the most important cause for the decrease in surface area when the porosity is increased from 0.494 to 0.551. It should be noted that the extent of the surface area does not only depend on diffusion and dispersion but also on the extent of the pore space, which is larger for higher porosity values.

3.2.3 Discussion on the porosity analysis

Our results show that changes in porosity do certainly have an influence on the movement of the solute through the pore network. However, in contrast to changes in flow rate, there seems to be no clear relation between porosity and the mean gradient and length of the solute frontline. An explanation for this is that changes in porosity do also affect other factors like pore radius distribution, pore coordination and blockage and the orientation of pores with the mean flow direction. These factors have a great influence on dispersion and therefore on the mean gradient and length of the concentration front (Sahimi et al, 1986). The graphs for a porosity of 0.435 and 0.494 look very different from the graphs for a porosity of 0.551, especially when looking at the time it takes for the solute to reach the end of the pore network. Further analysis of the raw experimental data has shown that this is most likely caused by an error that occurred during the experimental procedure. To get a good picture of the dependency of the front length and mean concentration gradient it is therefore necessary that these experiments will be repeated. These new experiments can then be done with a wider range in porosity values and can be a subject for further research.

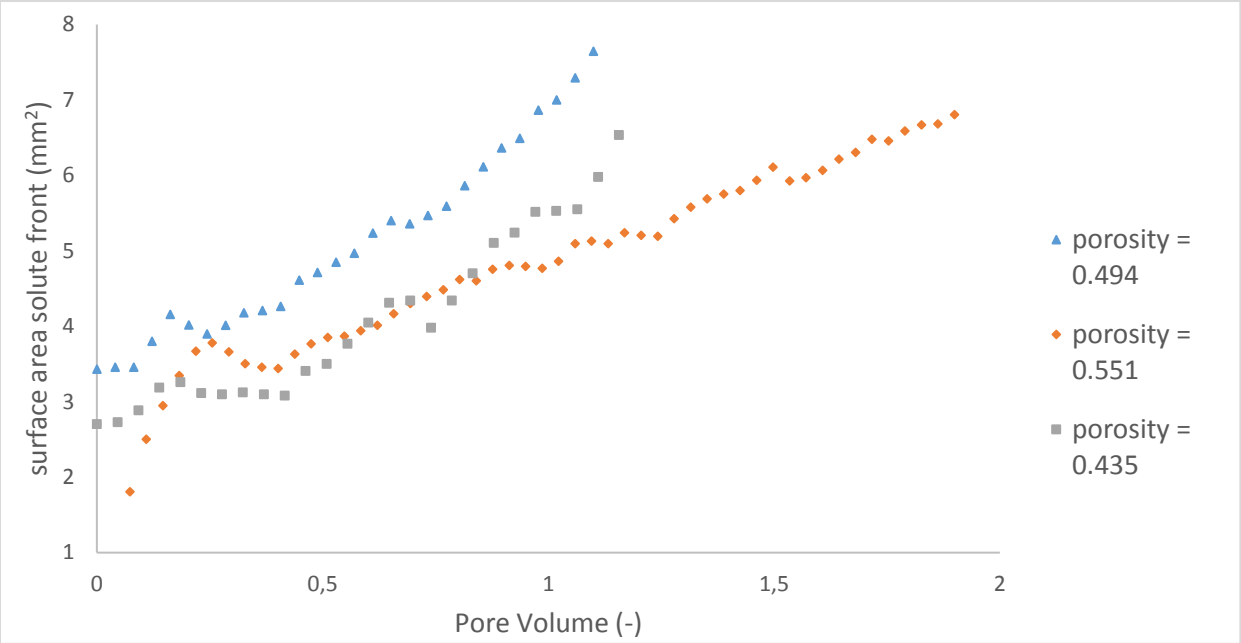

Figure 15. The surface area of the solute front for different porosities and a flow rate of 0.1 ml/hour plotted against Pore Volume.

4. Conclusion

For this research, images from micromodel experiments carried out by Raaijmakers (2018) have been used to analyze the dependency of the mean concentration gradient and frontline length of a solute front propagating through a saturated porous medium on flow rate and porosity. First, the images had to be filtered in order to remove noise. After that, the grey scale images were converted to concentration images using a relation between grey scale intensity and concentration. Paraview and Matlab software were used to obtain the solute frontline and the mean gradient of the solute front. Images from 5 different micromodel experiments with varying porosity and flow rate have been analyzed. Results of this analysis show that for all flow rates and a porosity of 0.551, the mean concentration gradients decrease with time due to diffusion until it reaches a constant state. Dispersion initially causes an increase in length of the solute frontline due to the forming of solute fingers. This increase ceases after some time because diffusion leads to merging of these solute fingers. An increase in flow rate leads to an increase of the maximum solute frontline length and an increase in mean concentration gradient as the solute reaches the end of the porous medium due to an increasing effect of dispersion over diffusion. Changes in porosity do affect the frontline length and the mean concentration gradient, although no clear relation between these variables have been found. In general, an increase in porosity leads to a smaller variability in particle velocity causing a decrease in dispersion. Also, the diffusion increases because the solute has more space to diffuse. These changes in diffusion and dispersion are reflected in a lower mean concentration gradient and a shorter solute frontline. However, analyze of the experimental data for different porosities did give some abnormal results that were most likely caused by an error that occurred during the experimental procedure.

This research has shown that image processing provides useful tools for analyzing data from micromodel experiments when it comes to the geometry of a propagating solute front through a saturated porous medium. Future research can focus on analyzing more different micromodels -i.e., more different porosity and flow rate values, and on optimizing the method of determining the solute frontline so that manual correction is no longer necessary.

Appendix

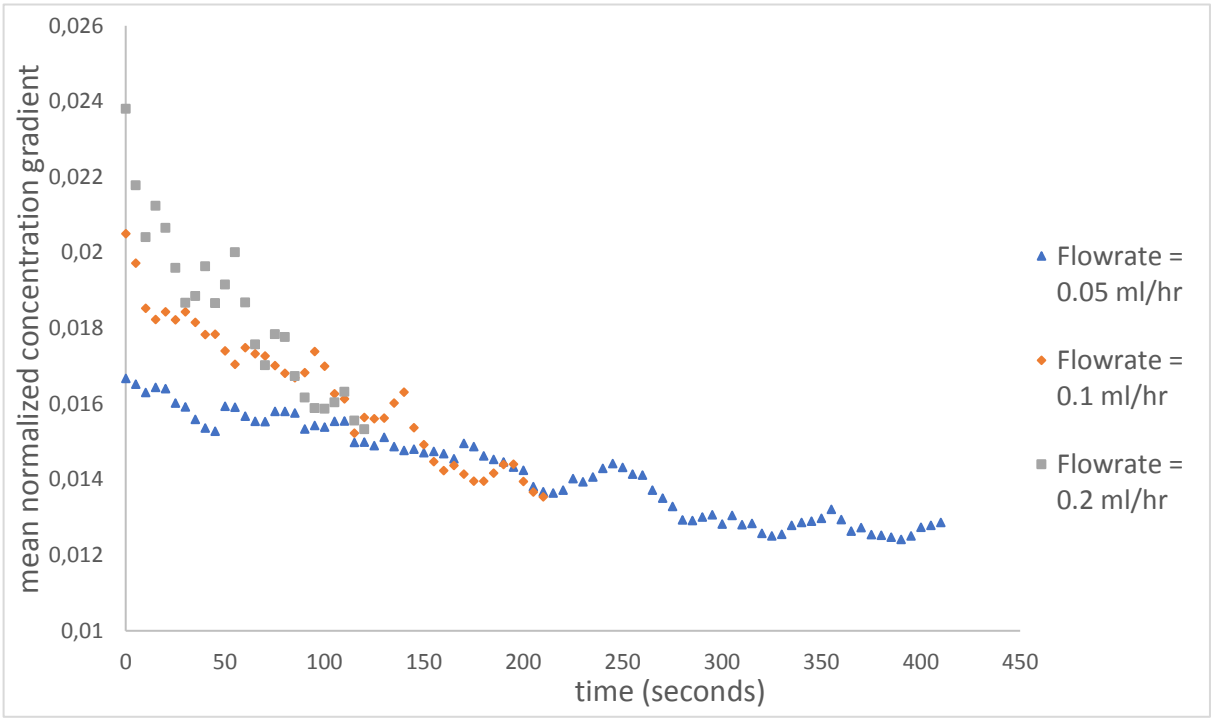
mean normalized concentration gradient
0,026
0,024
0,022
0,02
0,018
0,016
0,014
0,012
0,01
0
50
100
150
200
250
300
350
400
450
time (seconds)
Flowrate = 0.05 ml/hr
Flowrate = 0.1 ml/hr
Flowrate = 0.2 ml/hr

a.

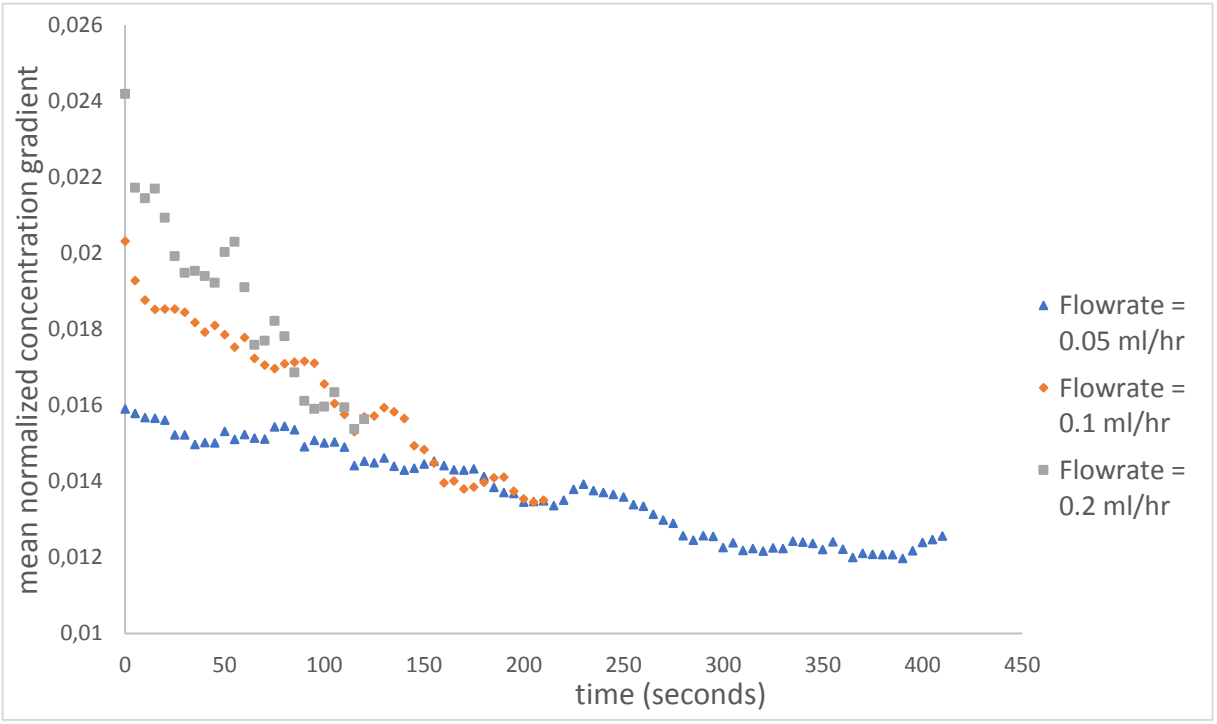
mean normalized concentration gradient
0,026
0,024
0,022
0,02
0,018
0,016
0,014
0,012
0,01
0
50
100
150
200
250
300
350
400
450
time (seconds)
Flowrate = 0.05 ml/hr
Flowrate = 0.1 ml/hr
Flowrate = 0.2 ml/hr

b.

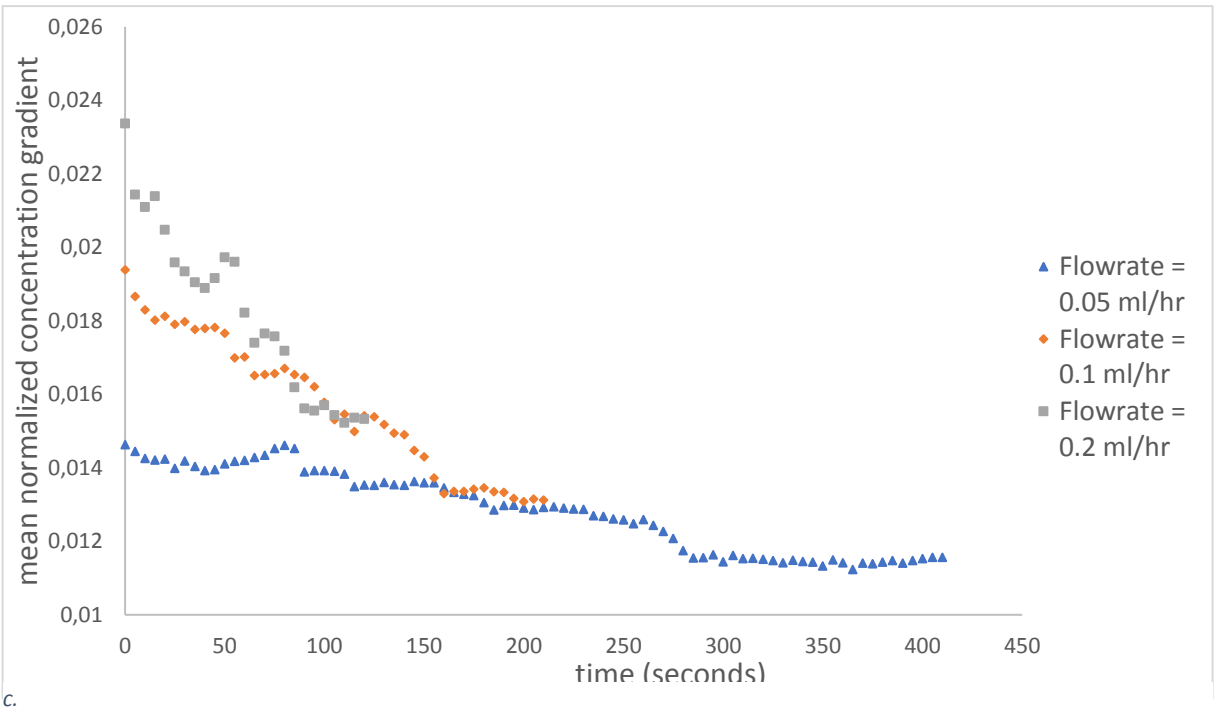

c.

Figure A1. *Mean normalized concentration gradients plotted against time for different flow rates. The concentration values that were defined as part of the front are from 0.4 to 0.6 for Figure a, from 0.3 to 0.6 for Figure b and from 0.2 to 0.6 for Figure c.*

References

Anna, P. D., Jimenez-Martinez, J., Tabuteau, H., Turuban, R., Le Borgne, T., Derrien, M., & Méheust, Y. (2013). Mixing and reaction kinetics in porous media: An experimental pore scale quantification. *Environmental science & technology*, *48*(1), 508-516.

Bear, J. (1988), *Dynamics of Fluids in Porous Media*, Dover, New York.

Bear, J., & Cheng, A. H. D. (2010). *Modeling groundwater flow and contaminant transport* (Vol. 23). Springer Science & Business Media.

Chatenever, A., & Calhoun Jr, J. C. (1952). Visual examinations of fluid behavior in porous media-part i. *Journal of Petroleum Technology*, *4*(06), 149-156.

Chen, D., Pyrak-Nolte, L. J., Griffin, J., & Giordano, N. J. (2007). Measurement of interfacial area per volume for drainage and imbibition. *Water Resources Research*, *43*(12).

Cheng, J. T. (2002). *Fluid flow in ultra-small capillaries* (Doctoral dissertation, Ph. D. Thesis, Purdue Univ., Lafayette, Indiana).

Cheng, J. T., Pyrak-Nolte, L. J., Nolte, D. D., & Giordano, N. J. (2004). Linking pressure and saturation through interfacial areas in porous media. *Geophysical Research Letters*, *31*(8).

Dentz, M., Le Borgne, T., Englert, A., & Bijeljic, B. (2011). Mixing, spreading and reaction in heterogeneous media: A brief review. *Journal of contaminant hydrology*, *120*, 1-17.

Ferreira, T., & Rasband, W. (2012). ImageJ user guide. *ImageJ/Fiji*, *1*.

Freeze, R. A., & Cherry, J. A. (1979). Groundwater, 604 pp.

Gramling, C. M., Harvey, C. F., & Meigs, L. C. (2002). Reactive transport in porous media: A comparison of model prediction with laboratory visualization. *Environmental science & technology*, *36*(11), 2508-2514.

Jiménez-Martínez, J., Anna, P. D., Tabuteau, H., Turuban, R., Borgne, T. L., & Méheust, Y. (2015). Pore-scale mechanisms for the enhancement of mixing in unsaturated porous media and implications for chemical reactions. *Geophysical Research Letters*, *42*(13), 5316-5324.

Joe Yeh, 2016 The vtkwrite script on the official Matlab website

Karadimitriou, N. K., & Hassanizadeh, S. M. (2012). A review of micromodels and their use in two-phase flow studies. *Vadose Zone Journal*, *11*(3).

Karadimitriou, N. K., Musterd, M., Kleingeld, P. J., Kreutzer, M. T., Hassanizadeh, S. M., & Joekar-Niasar, V. (2013). On the fabrication of PDMS micromodels by rapid prototyping, and their use in two-phase flow studies. *Water Resources Research*, *49*(4), 2056-2067.

Karadimitriou, N. K., Joekar-Niasar, V., Babaei, M., & Shore, C. A. (2016). Critical role of the immobile zone in non-Fickian two-phase transport: A new paradigm. *Environmental science & technology*, *50*(8), 4384-4392.

Kohl, S. K., Landmark, J. D., & Stickle, D. F. (2006). Demonstration of absorbance using digital color image analysis and colored solutions. *Journal of Chemical Education*, *83*(4), 644.

Pyrak-Nolte, L. J., Nolte, D. D., Chen, D., & Giordano, N. J. (2008). Relating capillary pressure to interfacial areas. *Water Resources Research*, *44*(6).

Raaijmakers, B. (2018). Solute transport in porous media; An experimental pore-scale study using physical micromodels. MSc Thesis. Utrecht University

Rasband, W. S. (1997). ImageJ. US National Institutes of Health, Bethesda, MD, USA.

Sahimi, M., Hughes, B. D., Scriven, L. E., & Davis, H. T. (1986). Dispersion in flow through porous media—I. One-phase flow. *Chemical engineering science*, *41*(8), 2103-2122.

Willingham, T. W., Werth, C. J., & Valocchi, A. J. (2008). Evaluation of the effects of porous media structure on mixing-controlled reactions using pore-scale modeling and micromodel experiments. *Environmental science & technology*, *42*(9), 3185-3193.

Xu, M., & Eckstein, Y. (1997). Statistical analysis of the relationships between dispersivity and other physical properties of porous media. *Hydrogeology Journal*, *5*(4), 4-20.